AD-A189 893 IMAGE CHARGE COHERENT SCATTERING AND SYMMETRY EFFECTS IN ELECTRON STIMULA..(U) GEORGE WASHINGTON UNIV WASHINGTON D C DEPT OF CHEMISTRY D E RAMAKER ET AL. 1/1

UNCLASSIFIED DEC 87 TR-38 N00014-80-K-0852 F/G 7/2 NL

[redacted]

END
DATE FILMED
3 88
DTIC

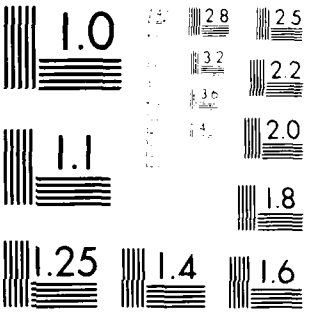
1.0
1.1
1.25
1.4
1.6
1.8
2.0
2.2
2.5
2.8
3.2
3.6

AD-A189 093

OFFICE OF NAVAL RESEARCH

Contract N00014-80-K-0852

R&T Code_____

Technical Report No. 38

Image Charge, Coherent Scattering, and Symmetry Effects in Electron Stimulated Desorption: O^- from O_2 Condensed on Metals

By

David E. Ramaker and Hideo Sambe

Prepared for Publication

in the

Desorption Induced by Electronic Transitions, DIET III
(Springer Series in Surface Science)

George Washington University
Department of Chemistry
Washington, D.C. 20052

December, 1987

(4)

SECURITY CLASSIFICATION OF THIS PAGE

REPORT DOCUMENTATION PAGE

1a. REPORT SECURITY CLASSIFICATION: Unclassified	1b. RESTRICTIVE MARKINGS
2a. SECURITY CLASSIFICATION AUTHORITY	3. DISTRIBUTION/AVAILABILITY OF REPORT: Approved for public release; distribution unlimited
2b. DECLASSIFICATION/DOWNGRADING SCHEDULE	
4. PERFORMING ORGANIZATION REPORT NUMBER(S): Technical Report #38	5. MONITORING ORGANIZATION REPORT NUMBER(S)
6a. NAME OF PERFORMING ORGANIZATION: Dept. of Chemistry, George Washington Univ. / 6b. OFFICE SYMBOL (If applicable)	7a. NAME OF MONITORING ORGANIZATION: Office of Naval Research (Code 413)
6c. ADDRESS (City, State, and ZIP Code): Washington, D.C. 20052	7b. ADDRESS (City, State, and ZIP Code): Chemistry Program, 800 N. Quincy Street, Arlington, Virginia 22217
8a. NAME OF FUNDING/SPONSORING ORGANIZATION: Office of Naval Research / 8b. OFFICE SYMBOL (If applicable)	9. PROCUREMENT INSTRUMENT IDENTIFICATION NUMBER: Contract N00014-80-K-0852
8c. ADDRESS (City, State, and ZIP Code): Chemistry Program, 800 N. Quincy, Arlington, VA 22217	10. SOURCE OF FUNDING NUMBERS: PROGRAM ELEMENT NO. 61153N; PROJECT NO. RR 013-08; TASK NO. PP013 08-01; WORK UNIT ACCESSION NO. NR 056-681
11. TITLE (Include Security Classification): Image Charge, Coherent Scattering, and Symmetry Effects in Electron Stimulated Desorption: O^- from O_2 Condensed on Metals (Unclassified)	
12. PERSONAL AUTHOR(S): D.E. Ramaker and H. Sambe	
13a. TYPE OF REPORT: Interim Technical / 13b. TIME COVERED: FROM _____ TO _____	14. DATE OF REPORT (Year, Month, Day): December 1987 / 15. PAGE COUNT: 8
16. SUPPLEMENTARY NOTATION: Prepared for publication in Desorption Induced by Electronic Transitions, DIET III, (Springer Series in Surface Science)	
17. COSATI CODES: FIELD / GROUP / SUB-GROUP	18. SUBJECT TERMS (Continue on reverse if necessary and identify by block number): Electron Stimulated Desorption; Image Charge; Coherent Scattering

19. ABSTRACT (Continue on reverse if necessary and identify by block number)

In this work we shall examine "Environmental" effects, which do not arise from alteration of the excited-state lifetime, but rather from. (1) the image charge induced in the metal substrate, (2) adsorbate-adsorbate interactions which reduce the symmetry and hence cause certain selection rules to breakdown, and (3) coherent scattering of electrons in the substrate. We review previously reported ESD yields of O^- from O_2 condensed on polycrystalline Pt in the electron energy range 0 to 40 eV.

20. DISTRIBUTION/AVAILABILITY OF ABSTRACT: ☒ UNCLASSIFIED/UNLIMITED ☒ SAME AS RPT. ☐ DTIC USERS	21. ABSTRACT SECURITY CLASSIFICATION: Unclassified
22a. NAME OF RESPONSIBLE INDIVIDUAL: Dr. David L. Nelson	22b. TELEPHONE (Include Area Code): (202) 696-4410 / 22c. OFFICE SYMBOL

DTIC ELECTE JAN 07 1988 E

DD FORM 1473, 84 MAR — 83 APR edition may be used until exhausted. All other editions are obsolete.

SECURITY CLASSIFICATION OF THIS PAGE: Unclassified

Image Charge, Coherent Scattering, and Symmetry Effects in Electron Stimulated Desorption: O^- from O_2 Condensed on Metals

David E. Ramaker and Hideo Sambe
Department of Chemistry, George Washington University
Washington, DC 20052, USA

1. Introduction

Considerable progress has been made towards our understanding of electron/photon stimulated desorption (ESD/PSD) [1]. Identification of the excited states responsible for desorption reveals that they usually are many particle excitations (i.e. n holes (h)-n electrons (e), such 2h, 2h-1e etc.) and arise from widely different excitation mechanisms [2]. Furthermore, it is known that the lifetime of these localized excitations, which determine the probability for desorption, is very much altered by covalent interactions between the active site and its immediate environment [3]. In this work we shall examine "environmental" effects, which do not arise from alteration of the excited-state lifetime, but rather from: (1) the image charge induced in the metal substrate, (2) adsorbate-adsorbate interactions which reduce the symmetry and hence cause certain selection rules to breakdown, and (3) coherent scattering of electrons in the substrate.

We review previously reported [4] ESD yields of O^- from O_2 condensed on polycrystalline Pt in the electron energy range 0 to 40 eV. Of the various species which may desorb (O^-, O, and O^+), O^- desorption is the most convenient to study here for three reasons: 1) the O^- desorption yields appear to be dominated by resonant ESD processes, thus the O^- yields are easier to interpret quantitatively than the non-resonant ESD O^+ yields; 2) the ESD O^- yields are about as straightforward to interpret as PSD O^+ yields, but they do not require use of a synchrotron for measurement; and 3) the O yields are more difficult to observe experimentally, and they may have contributions from both resonant and nonresonant mechanisms making them more complex to interpret [2,5].

The apparatus utilized to obtain the experimental data described here has been described previously [6], and it is also fully described in the article by Sanche in this volume. The incident angle of the electron beam is 20° from the surface, and the O^- ions are measured by a quadrapole mass spectrometer positioned at 70° from the surface. The film thicknesses are estimated to within 20% by a method described previously [6]. A rare gas (RG) is condensed near its sublimation temperature on a clean Pt ribbon, and the O_2 gas is condensed onto the RG film at 17 K. Electron Transmission Spectra (ETS) data [7] reveal that the RG films are essentially ordered, since Bragg reflection (BR) minima are observed around 5 and 9 eV for Ar, 4, 7, and 9 eV for Kr, and 2.5, 5, and 7.5 for Xe. In contrast, Xe films prepared well below the sublimation temperature do not exhibit BR minimum in ETS [7]. Data also indicate that the Ar films seem to be more ordered than the Kr and Xe films [8].

The three different "environmental" effects under study in this review, can be isolated in the O^- yields from O_2/RG/Pt system. The effects of ion neutralization are minimized by inserting a rare gas (Ar, Kr, or Xe) layer between the Pt metal and the O_2 layer. The RG layer also serves as a spacer layer so that the distance between the ion and the metal surface can be varied, thus varying the effect of the image charge force on the desorbing ions [4]. The image charge effects are best studied for O_2(0.16 ML)/RG(1-6 ML)/Pt. Adsorbate-adsorbate interactions become important at larger O_2 coverages when symmetry breakdown effects become visible. Finally, in the range O_2(0.16 ML)/RG(6-35 ML)/Pt, coherent scattering effects dominate.

Figure 1 compares the electron-energy dependence of the ESD O^- yield from O_2(.1 ML)/Ar(1-32 ML)/Pt as a function of incident electron energy. The electron impact O^- dissociation of O_2 gas is well understood [9]. In the energy range from 4.4 to 10 eV, the O^- ions are produced via the transient $O_2^-(^2\Pi_u)$ anion in a process referred to as dissociative attachment (DA). Above 17 eV, the O^- ions are produced predominantly via an excited neutral O_2^* molecule in a process referred to as dipolar dissociation (DD).

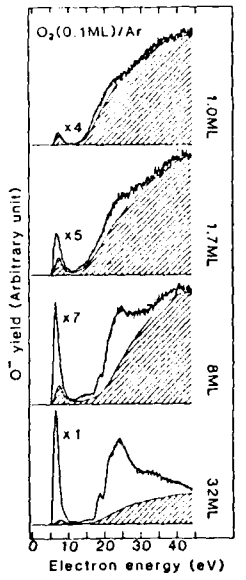

Fig. 1 Comparison of the ESD O^- yield curves obtained from O_2/Ar/Pt with a constant (0.1 ML) O_2 coverage and variable (1-32 ML) Ar thicknesses [4]. The shaded areas indicate the estimated contributions due to the direct process.

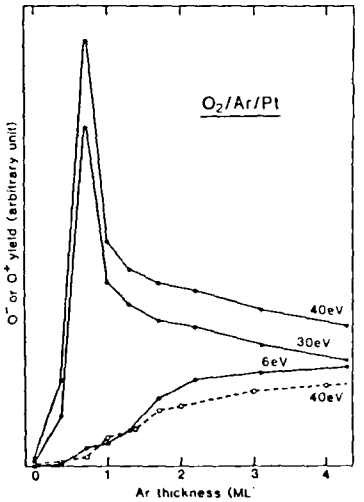

Fig. 2. Ar thickness dependence of the O^- yields produced by ESD from the O_2/Ar/Pt samples with a constant (0.1 ML) O_2 coverage [4]. The incident electron energies are as indicated. Also shown (dotted curve) is the O^+ yield produced by ESD with incident energy of 40 eV on O_2(0.16 ML)/Ar(variable)/ Pt [4].

2. Image Charge Effects

Fig. 2 shows the Ar thickness dependence of the O^- yield from O_2/Ar/Pt with a constant (0.1 ML) O_2 coverage. The sharp maximum probably corresponds to the case when the Ar plus O_2 coverage form one ML to within experimental uncertainty. Fig. 2 also shows the O^+ yield from O_2(0.16 ML)/Ar(variable)/Pt samples produced by 40-eV electron impact. In O_2 gas, O^+ formation by 40-eV electron impact arises predominantly via an O_2^+ intermediate state [10]. Therefore, we expect that both the O^+ yield and the DA contribution to the O^- yield are produced via charged intermediate states, O_2^+ and O_2^-, respectively. Fig. 2 shows that the image charge has a similar effect on these charged states and their dissociated ions.

Four effects that the image charge has on the desorption yield can be summarized using the semi-quantitative, adiabatic potential energy curves for O_2 depicted in Fig. 3 [4]. The solid curves give the ground state of O_2, the $^2\Pi_u$ O_2^- state and its partner dissociating to the lowest O^-+O limit, and a O_2^+ state and its partner dissociating to *the lowest* O^++O^- *limit* [4]. The two O_2^- and two O_2^+ states each form a pair of states which at large separation have

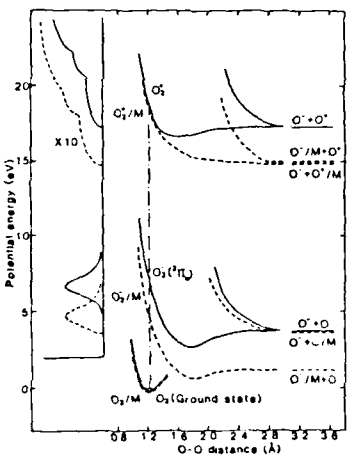

Fig. 3 Potential energy curves of O_2 gas (solid curves), and the *corresponding* potential energy curves under the influence of an image charge (dotted curves). Spectra on the *left* side show schematically the *relative number of* vibrational and/or electronic states which have sufficient energy to yield O^- ions, for O_2 gas (solid lines) and for O_2/M (dotted lines) [4].

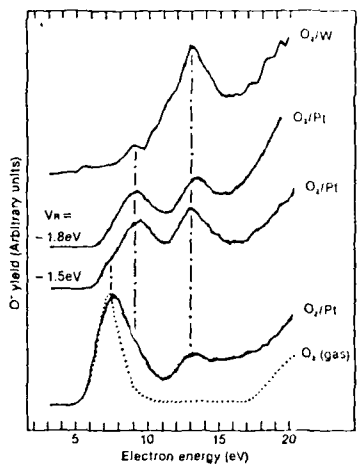

Fig. 4 Comparison of the O^- yields from O_2 gas with that from O_2(3 ML)/Pt at 17 K [14] (with retarding potentials of V_R = 0, -1.5, and -1.8 eV), and from O_2(1 ML)/W at 300 K [15].

wavefunctions approaching $[\psi(O_a^-)\psi(O_b) \pm \psi(O_a)\psi(O_b^-)]$ and $[\psi(O_a^+)\psi(O_b^-) \pm \psi(O_a^-)\psi(O_b^+)]$ respectively, where $\psi(O_a)$ denotes the wavefunction for an isolated O atom at site "a". The dotted curves give the corresponding potential energy curves in the presence of the image charge. The symbol O^+/M in Fig. 3, for example, means that the O^+ ion is near a metal surface. The image charge due to the Pt lowers the energies of the ionic species such as O^+/M, O^-/M, and O_2^-/M, while the energies of the neutral species such as O/M, O_2^*/M and O_2/M remain the same. The magnitude of this lowering depends on the distance between the ion and the metal surface, and hence on the thickness of the rare gas spacer layer. The curves in Fig 3 are drawn assuming the maximum energy lowering, 2.5 eV [4].

The first effect of the image charge involves the energy separation of the O + O^- dissociation limit into the O/M+O^- and O^-/M+O limits. Consequently, to desorb O^- ions, the lower O_2^-/M intermediate state must undergo a non-radiative transition into its upper partner state. The mechanism for this "charge transfer" transition, O^-/M+O to O/M+O^-, is similar to that for symmetric charge transfer in atom-atom collisions of identical nuclei [11] and occurs because of the breakdown of the adiabatic approximation. The probability for this transition is 1/2 when the separation of the dissociation limits vanishes, and decreases quickly as the separation increases. In contrast, the separation between the $O^-/M+O^+$ and O^-+O^+/M dissociation limits is negligibly small. Nevertheless, based on the relative atomic sizes of O^+ and O^-, we expect that the O^-+O^+/M limit is slightly lower than the $O^-/M+O^+$ limit. This means that the DA contribution should increase and the DD contribution should decrease slightly as the thickness of the rare gas layer increases.

The second effect of the image charge involves the kinetic energy of the escaping O^- ions. As can be seen easily in Fig. 3, in comparison with the *corresponding* O^- kinetic energy from O_2 gas, the kinetic energy of the O^- ions via O_2^-/M is decreased while that via O_2^*/M is increased. The slower escaping ions have a greater chance to be recaptured or neutralized, thus decreasing the DA O^- yield, while the faster O^- ions have a greater chance for escape, thus increasing the DD O^- yield. However, this mechanism probably causes a relatively small effect.

The third effect of the image charge involves the number of vibrational and/or electronic intermediate states (*i.e., amount of configuration space*) which have sufficient energy to yield O^- ions. The curves on the left side of Fig. 3 schematically indicate the configuration space for production of O^- from O_2 gas (solid lines) and from O_2/M (dotted lines). These plots indicate that the configuration space for O_2^-/M decreases slightly while that for the O_2^*/M state increases significantly compared to that for O_2.

Finally, the fourth effect of the image charge involves the quenching rate of the intermediate state. Near a metal surface, some of the O_2^- or O_2^* states may be neutralized or de-excited before the desorption process can get underway. The image charge influences these destruction rates of the O_2^- intermediate state by attracting the ion towards the metal surface. The inward motion and subsequent neutralization are similar to the first two steps of the Antoniewicz "bounce" mechanism [12], which is known to be active for neutral desorption from physisorbed systems [13]. Again in contrast, the de-excitation rate of the O_2^* intermediate state is not affected by the image charge. Thus, intermediate state quenching has a greater effect on the DA process than on the DD process.

All four image charge mechanisms predict a depletion of the DA process relative to the DD process. This is consistent with the two-orders of magnitude reduction seen in the O^-(via DA)/O^-(via DD) ratio for the O_2(0.37 ML)/Ar/Pt system compared with that of O_2 gas. As the thickness of the rare gas spacer layer decreases from 4 to 1 ML, the image charge force increases. Accordingly, with decreasing rare gas thickness, the O^- yield via the DA process should decrease and that via the DD process should increase. This is consistent with Fig. 2. As indicated above, the dissociation branching effect for the DA process, and the configuration space effect for the DD process, are primarily responsible for this behavior.

3. Symmetry Effects

Figure 4 compares the O^- yield from O_2 gas with that from O_2(3 ML)/Pt at 17 K [14] and O_2 (1 ML)/W at 300 K [15] in the electron energy range 2-20 eV, i.e. in the range where the DA contribution dominates. The data for O_2/Pt is also shown with retarding potentials, V_R, of -1.5 and -1.8 eV. These later data provide a measure of the kinetic energy of the desorbing O^-, since only ions in excess of V_R can be collected. Note that application of the retarding potentials for O_2/Pt eliminates the 7 ev peak, making it comparable to that for O_2/W. The data also reveal the presence of peaks around 9 and 13 eV in the O^- yields from the chemisorbed systems, which are absent for O_2.

A theoretical analysis [16] indicates that the 9 and 13 eV features arise from the $^2\Sigma_g^+$ and $^2\Sigma_u^+$ resonances which have excitation energies in this region. These two Σ^+ resonances do not appear in the yield from O_2 because of a selection rule which does not allow $\Sigma^- \rightarrow \Sigma^+$ transitions from the $^3\Sigma_g^-$ ground state of O_2 in the gas phase, or even at low coverages on the RG/Pt substrate [16]. However at higher coverages, O_2-O_2 interactions on the surface, and perhaps even dimer formation, causes this selection rule to break down [16].

Image charge effects are responsible for the remaining differences seen in Fig. 4. The principal $^2\Pi_u$ DA contribution at 7 eV is absent in the yield from O_2/W primarily because of the branching ratio mechanism described above. It is present in the yield from O_2/Pt at the 3 ML O_2 thickness because the image charge effect is already decreased. The retarding potentials of 1.5 and 1.8 eV eliminate this contribution because the $^2\Pi_u$ resonance apparently produces O^- of kinetic energy less than these energies while the O^- from the two $^2\Sigma^+$ resonances have larger kinetic energies [14]. Although the image charge via the branching ratio mechanism essentially eliminates the $^2\Pi_u$ contribution, it increases the two $^2\Sigma^+$ contributions because these two resonances correlate to the upper O/M + O^- dissociation limits, while their partner states (the $^2\Sigma_u^+$ and $^2\Sigma_g^+$) correlate to the lower O + O^-/M dissociation limits [16]. Thus the image charge effect can increase or decrease the DA yield depending on whether the excited resonance correlates to the upper or lower limit.

The data and interpretation above provides an answer to the long standing question concerning the active sites for O_2/W; i.e. are they atomic or molecular sites [17]. The presence of the two $^2\Sigma^+$ resonance contributions and the similarity of the DD contributions for O_2/W and O_2 gas clearly indicate that the minority molecular sites are the active ones in this case. However, the O^- yields from O_2(1 ML)/Mo at 300 K [15] suggests that both the molecular and the atomic sites are active, because spectral features in the total yield align with those from O_2/W and from the OH^a yield from OH/TiO_2 [5]. Portions of the OH^a yield have been shown to arise from the DA mechanism, and

therefore must involve breaking O-Ti bonds, i.e. the OH^a spectral lineshape should mimic the O^- spectral lineshape from atomic O sites on Pt [5]. A least squares fit of the O^- from O_2/W and OH^a from OH/TiO_2 spectral lineshapes to the O^- yield from O_2/Mo suggest that about half of the O^- yield from O_2/Mo arises from the minority molecular sites and half from the predominant atomic sites [16].

4. Coherent Scattering Effects

Fig. 1 shows that for O^- from O_2/Ar(1-32 ML)/Pt, the three features at 6, 18, and 24 eV grow faster than the remainder of the spectrum, and at large thicknesses (>20 ML) dominate the spectrum [4]. The O^- yields at these three energies are plotted as a function of the Ar thickness in Fig. 5. The spectral shape of the 6-eV feature depends on the RG, the thickness and structural order of the RG layer, and the O_2 coverage. It is broad and symmetric at small RG thicknesses but sharp, asymmetric, and shifted to lower energy at larger thicknesses. It is much narrower at smaller O_2 coverages than at larger coverages (Fig. 6). The dependence on the RG and on the structural order of the RG can also be seen in Fig. 6 [4].

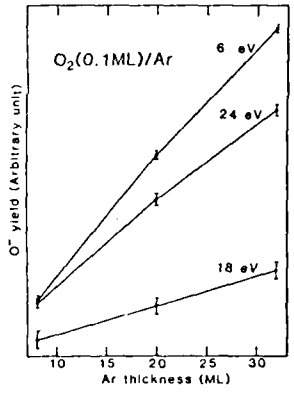

Fig. 5 Ar thickness dependence of the ESD O^- yields from O_2(0.1 ML)/Ar/Pt [4]. The incident electron energies are as indicated.

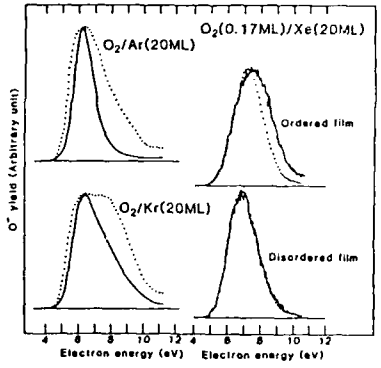

Fig. 6 LEFT) Comparison of the ESD O^- yield curves obtained with a constant rare gas (Ar or Kr) thickness (20 ML) but with different O_2 coverages, 0.03 ML (solid curves) and 1.0 ML (dotted curves)[4]. RIGHT) ESD O^- yield curves obtained from O_2(0.1 ML)/Xe(20 ML)/Pt but prepared at 40 K (top) and 17 K (bottom). Also shown are ESD O^- yield curves from O_2 gas (dotted curves) [4].

The experimental results described above can be explained in terms of three processes which we call the direct (D), elastic-indirect (EID), and inelastic-indirect (IID) processes [4]. In the D process, an incident electron collides with an O_2 on the surface and produces an O^- directly. In the EID process, an incident electron at an energy below the first electronic excitation energy (first E_{ex}) of the RG, passes through the O_2 layer without loss of energy, undergoes quasi-elastic multiple scattering in the RG, and returns to the surface, where it collides with an O_2 and produces O^- as in the D process. The IID process is identical to the EID, except that the electron upon initial entry into the RG film suffers loss of energy by electronically exciting the RG. At electron energies above the first E_{ex}, the inelastic mean free path in RG films is very short (≈ 10 A° [4]).

The O^- yield via these processes are proportional to the following expressions [4],

$$\begin{aligned} D &= \Theta\ \sigma(E) \\ EID &= [1-\Theta\ \sigma_{el}(E)]\ P_s(RG,\tau,E)\ \Theta\ \sigma(E), \\ IID &= [1-\Theta\ \sigma_{el}(E)]\ P_{ex}(RG,E_{ex},E)\ \ P_s(RG,\tau,E-E_{ex})\ \ \Theta\ \sigma(E-E_{ex}). \end{aligned} \qquad (1)$$

Here, E denotes the incident electron energy, Θ the O_2 coverage, and $\sigma(E)$ the O^- yield cross section from O_2 on the RG film. $\sigma(E)$ is assumed to be independent of the RG thickness beyond 7 ML. The $[1-\Theta\ \sigma_{el}(E)]$ factor gives the probability of passing through the O_2 layer without loss of energy, where $\sigma_{el}(E)$ is equal to a sum of the elastic backscattering and the total inelastic cross sections of O_2. $P_s(RG,\tau,E)$ denotes the probability of the electron returning to the surface, which depends on the RG, the RG thickness (τ), and the electron energy in the film. $P_{ex}(RG,E_{ex},E)$ denotes the electronic excitation probability of the RG film by electron impact at energy E. Since $\sigma_{el}(E)$ and $P_{ex}(E)$ are slowly varying functions of E [4], the E dependence of the D, EID, and IID contributions are primarily determined by $\sigma(E)$ and $P_s(E)$. Because of the short inelastic mean free path, the O^- yield, $Y(RG,t,E)$, below and above the first E_{ex} are given by $Y = D + EID$ and $Y = D + IID$, respectively.

Figure 5 shows that the O^- yields at 6, 18, and 24 eV all increase as the Ar layer thickness increases [4]. Equation (1) indicates that this relationship exists because of the two indirect processes. The 6, 18 and 24 eV features observed for O_2(0.1 ML)/Ar(32 ML) arise predominantly from the EID, IID, and IID processes respectively. The spectral shape of $\sigma(E)$, or the D contribution, is expected to be similar to the O^- yield from O_2 gas except for the relative magnitude of the DA and DD contributions. Polarization of the thick RG layer reduces the O^- yield via the DA process, but enhances that via the the DD process, compared with that for O_2 gas . Our estimates of the D contribution, indicated in Fig. 1 by the shaded areas, are based on the above considerations. The intensity ratio EID/D for O_2(0.1 ML)/Ar(32 ML) is about 70 at the peak energy of the 6-eV feature which means that P_s is around 90. For thicker and more ordered Ar films, we expect even larger values of P_s. Since the maximum P_s obtainable by incoherent multiple scattering is around 2, coherent scattering must be playing a dominant role.

The spectral shape of the 6-eV feature for the different RG films can be correlated with the BR minima observed in ETS data. The 6-eV line shape from a disordered Xe film is virtually identical with that from O_2 gas (Fig. 6). Since $\sigma(E)$ is virtually identical in the 5-10 eV range with that from O_2 gas, $P_s(E)$ for the disordered film must be nearly invariant with E over this same

energy range. However, $P_s(E)$ for the ordered film must vary over this energy range, since the line shape of the ordered Xe film differs from that for O_2 gas (Fig. 6). The 6-eV line shape for Ar also depends on the O_2 coverage so that at the lower coverage (0.03 ML), it is narrower than $\sigma(E)$ and its peak is shifted to lower energy (Fig. 1 and 6). All these suggest that $P_s(E)$ for Ar is strongly enhanced near the first BR minimum around 5 eV. The peak for Kr at the lower O_2 coverage is also shifted to lower energy (Fig. 6); however, the line shape is wider than $\sigma(E)$ apparently because two BR energies (4 and 7 eV) partially overlap with $\sigma(E)$. The O^- yield is enhanced for Ar more strongly than for Kr, because the first BR minimum for Ar is closer to the peak of $\sigma(E)$, and perhaps also because the Ar film is more ordered. This analysis indicates that $P_s(E)$ is enhanced near BR energies, especially strongly near the first BR minimum [4].

It is well known that for a perfect crystal the electronic wavefunctions just above and below the energy band gaps, which arise from the BR's, have standing-wave character [18]. We conclude that this standing-wave character is responsible for the large enhancement of P_s near the BR energies. The increase of P_s with RG thickness is also consistent with this since the standing-wave character should increase with RG thickness. However, this raises an interesting question. How does a relatively small increase in the amplitude of the electronic wavefunction (i.e. at most a factor of 2 due to the standing-wave character) cause such a dramatic increase in the O^- desorption yield (a factor of 10^2)? Clearly, either some quantum mechanical matrix element effect causes the $O_2 \rightarrow O_2^-$ cross-section to increase non-linearly with standing-wave character, or the $O_2 \rightarrow O^-$ desorption branching ratio increases with standing-wave character. These possibilities must still be investigated.

5. Summary

In this work we have observed the following environmental effects: 1) the image charge causes desorption yields arising from neutral intermediates to increase, while those arising from ionic intermediates may decrease or increase depending on the dissociation limit of the ionic intermediate state, 2) O_2-O_2 interaction effects at the surface reduce the local symmetry, cause a breakdown in the $\Sigma^- \nrightarrow \Sigma^+$ selection rule, and thus introduce additional dissociative attachment contributions in the O^- yield, and 3) coherent scattering in the rare gas may enhance the O^- yield up to two orders of magnitude near the Bragg reflection energies. The observed image charge and adsorbate-adsorbate interaction effects should be generally observed in other systems. The coherent scattering effects will be large only for low energy desorption thresholds when the inelastic mean free path of the electrons is long. This explains why X^+ desorption, which generally has higher energy thresholds, may be less affected by coherent scattering and hence has not exhibited these large effects to date.

Acknowledgements

We have greatly benefited from discussions with Leon Sanche. This work was supported in part by the Office of Naval Research.

References

1. a) Desorption Induced by Electronic Transitions DIET I, ed. by N.H. Tolk, M.M. Traum, J.C. Tully, and T.F. Madey, Springer Ser. Chem. Phys., Vol. 24 (Springer, Berlin, Heidelberg 1983); b) Desorption Induced by Electronic Transitions DIET II, ed. by W. Brenig and D. Menzel, Springer Ser. Surf. Sci., Vol. 4 (Springer, Berlin, Heidelberg 1985).
2. D.E. Ramaker p. 70 in Ref. 1a and p. 10 in Ref. 1b above.
3. D.E. Ramaker J. Vac. Soc. Technol. A1, 1137 (1983).
4. H. Sambe, D.E. Ramaker, L. Parenteau, and L. Sanche: Phys. Rev. Lett. 59, 505 (1987), 59, 505 (1987).
5. R.L. Watson, D.E. Ramaker, V.M. Bermudez, and M.A. Hoffbauer: J. Vac. Sci. Technol. A3, 1675 (1985).
6. L. Sanche and L. Parenteau: J. Vac. Sci. Technol. A4, 1240 (1986).
7. G. Baier et al.: Phys. Rev. B30, 78 (1984); B26, 6019 (1982).
8. M. Fernandez et al.: Phys. Rev. Lett. 55, 545 (1985).
9. G.D. Schmidt: Rev. Mod. Phys. 45, 423 (1973); R. Locht and J. Momigny: Int. J. Mass Spectrom. Ion Phys. 7, 121 (1971); D. Rapp and D.D. Briglia: J. Chem. Phys. 43, 1480 (1965).
10. R. Locht and J. Schopman: Int. J. Mass Spectrom. Ion Phys. 15, 361 (1974), Chem. Phys. Lett. 26, 596 (1974).
11. S. Geltman, Topics in Atomic Collision Theory (Academic Press, New York, 1969).
12. P.R. Antoniewicz: Phys. Rev. B21, 3811 (1980).
13. F. Feulner et al.: Phys. Rev. Lett. 53, 671 (1984); Q.J. Zhang, R. Gomer, and D.R. Bowman: Surf. Sci. 129, 555 (1983).
14. H. Azria, L. Parenteau, and L. Sanche: to be published.
15. Z.X. Liu and D. Lichtman: Surf. Sci. 114, 287 (1982).
16. H. Sambe and D.E. Ramaker: to be published.
17. E. Bauer: p. 104 in Ref. 1a.
18. C. Kittel: "Introduction to Solid State Physics", 6th ed. (John Wiley & Sons, NY, 1986), Chap. 7.

TECHNICAL REPORT DISTRIBUTION LIST, GEN

	No. Copies
Office of Naval Research Attn: Code 1113 800 N. Quincy Street Arlington, Virginia 22217-5000	2
Dr. Bernard Douda Naval Weapons Support Center Code 50C Crane, Indiana 47522-5050	1
Naval Civil Engineering Laboratory Attn: Dr. R. W. Drisko, Code L52 Port Hueneme, California 93401	1
Defense Technical Information Center Building 5, Cameron Station Alexandria, Virginia 22314	12 high quality
DTNSRDC Attn: Dr. H. Singerman Applied Chemistry Division Annapolis, Maryland 21401	1
Dr. William Tolles Superintendent Chemistry Division, Code 6100 Naval Research Laboratory Washington, D.C. 20375-5000	1
Dr. David Young Code 334 NORDA NSTL, Mississippi 39529	1
Naval Weapons Center Attn: Dr. Ron Atkins Chemistry Division China Lake, California 93555	1
Scientific Advisor Commandant of the Marine Corps Code RD-1 Washington, D.C. 20380	1
U.S. Army Research Office Attn: CRD-AA-IP P.O. Box 12211 Research Triangle Park, NC 27709	1
Mr. John Boyle Materials Branch Naval Ship Engineering Center Philadelphia, Pennsylvania 19112	1
Naval Ocean Systems Center Attn: Dr. S. Yamamoto Marine Sciences Division San Diego, California 91232	1

DL/1113/87/2

ABSTRACTS DISTRIBUTION LIST, 056/625/629

Dr. F. Carter
Code 6170
Naval Research Laboratory
Washington, D.C. 20375-5000

Dr. Richard Colton
Code 6170
Naval Research Laboratory
Washington, D.C. 20375-5000

Dr. Dan Pierce
National Bureau of Standards
Optical Physics Division
Washington, D.C. 20234

Dr. R. G. Wallis
Department of Physics
University of California
Irvine, California 92664

Dr. D. Ramaker
Chemistry Department
George Washington University
Washington, D.C. 20052

Dr. J. C. Hemminger
Chemistry Department
University of California
Irvine, California 92717

Dr. T. F. George
Chemistry Department
University of Rochester
Rochester, New York 14627

Dr. G. Rubloff
IBM
Thomas J. Watson Research Center
P.O. Box 218
Yorktown Heights, New York 10598

Dr. J. Baldeschwieler
Department of Chemistry and
Chemical Engineering
California Institute of Technology
Pasadena, California 91125

Dr. Galen D. Stucky
Chemistry Department
University of California
Santa Barbara, CA 93106

Dr. A. Steckl
Department of Electrical and
Systems Engineering
Rensselaer Polytechnic Institute
Troy, New York 12181

Dr. John T. Yates
Department of Chemistry
University of Pittsburgh
Pittsburgh, Pennsylvania 15260

Dr. R. Stanley Williams
Department of Chemistry
University of California
Los Angeles, California 90024

Dr. R. P. Messmer
Materials Characterization Lab.
General Electric Company
Schenectady, New York 22217

Dr. J. T. Keiser
Department of Chemistry
University of Richmond
Richmond, Virginia 23173

Dr. R. W. Plummer
Department of Physics
University of Pennsylvania
Philadelphia, Pennsylvania 19104

Dr. E. Yeager
Department of Chemistry
Case Western Reserve University
Cleveland, Ohio 41106

Dr. N. Winograd
Department of Chemistry
Pennsylvania State University
University Park, Pennsylvania 16802

Dr. Roald Hoffmann
Department of Chemistry
Cornell University
Ithaca, New York 14853

Dr. Robert L. Whetten
Department of Chemistry
University of California
Los Angeles, CA 90024

Dr. Daniel M. Neumark
Department of Chemistry
University of California
Berkeley, CA 94720

Dr. G. H. Morrison
Department of Chemistry
Cornell University
Ithaca, New York 14853

ABSTRACTS DISTRIBUTION LIST, 056/625/629

Dr. J. E. Jensen
Hughes Research Laboratory
3011 Malibu Canyon Road
Malibu, California 90265

Dr. J. H. Weaver
Department of Chemical Engineering
and Materials Science
University of Minnesota
Minneapolis, Minnesota 55455

Dr. A. Reisman
Microelectronics Center of North Carolina
Research Triangle Park, North Carolina
27709

Dr. M. Grunze
Laboratory for Surface Science
and Technology
University of Maine
Orono, Maine 04469

Dr. J. Butler
Naval Research Laboratory
Code 6115
Washington D.C. 20375-5000

Dr. L. Interante
Chemistry Department
Rensselaer Polytechnic Institute
Troy, New York 12181

Dr. Irvin Heard
Chemistry and Physics Department
Lincoln University
Lincoln University, Pennsylvania 19352

Dr. F. J. Klaubunde
Department of Chemistry
Kansas State University
Manhattan, Kansas 66506

Dr. C. B. Harris
Department of Chemistry
University of California
Berkeley, California 94720

Dr. R. Bruce King
Department of Chemistry
University of Georgia
Athens, Georgia 30602

Dr. R. Reeves
Chemistry Department
Renssaeler Polytechnic Institute
Troy, New York 12181

Dr. Steven M. George
Stanford University
Department of Chemistry
Stanford, CA 94305

Dr. Mark Johnson
Yale University
Department of Chemistry
New Haven, CT 06511-8118

Dr. W. Knauer
Hughes Research Laboratory
3011 Malibu Canyon Road
Malibu, California 90265

Dr. Theodore E. Madey
Surface Chemistry Section
Department of Commerce
National Bureau of Standards
Washington, D.C. 20234

Dr. J. E. Demuth
IBM Corporation
Thomas J. Watson Research Center
P.O. Box 218
Yorktown Heights, New York 10598

Dr. M. G. Lagally
Department of Metallurgical
and Mining Engineering
University of Wisconsin
Madison, Wisconsin 53706

Dr. R. P. Van Duyne
Chemistry Department
Northwestern University
Evanston, Illinois 60637

Dr. J. M. White
Department of Chemistry
University of Texas
Austin, Texas 78712

Dr. Richard J. Saykally
Department of Chemistry
University of California
Berkeley, California 94720

DL/1113/87/2

ABSTRACTS DISTRIBUTION LIST, 056/625/629

Dr. G. A. Somorjai
Department of Chemistry
University of California
Berkeley, California 94720

Dr. J. Murday
Naval Research Laboratory
Code 6170
Washington, D.C. 20375-5000

Dr. W. T. Peria
Electrical Engineering Department
University of Minnesota
Minneapolis, Minnesota 55455

Dr. Keith H. Johnson
Department of Metallurgy and
Materials Science
Massachusetts Institute of Technology
Cambridge, Massachusetts 02139

Dr. S. Sibener
Department of Chemistry
James Franck Institute
5640 Ellis Avenue
Chicago, Illinois 60637

Dr. Arold Green
Quantum Surface Dynamics Branch
Code 3817
Naval Weapons Center
China Lake, California 93555

Dr. A. Wold
Department of Chemistry
Brown University
Providence, Rhode Island 02912

Dr. S. L. Bernasek
Department of Chemistry
Princeton University
Princeton, New Jersey 08544

Dr. W. Kohn
Department of Physics
University of California, San Diego
La Jolla, California 92037

Dr. Stephen D. Kevan
Physics Department
University Of Oregan
Eugene, Oregon 97403

Dr. David M. Walba
Department of Chemistry
University of Colorado
Boulder, CO 80309-0215

Dr. L. Kesmodel
Department of Physics
Indiana University
Bloomington, Indiana 47403

Dr. K. C. Janda
University of Pittsburg
Chemistry Building
Pittsburg, PA 15260

Dr. E. A. Irene
Department of Chemistry
University of North Carolina
Chapel Hill, North Carolina 27514

Dr. Adam Heller
Bell Laboratories
Murray Hill, New Jersey 07974

Dr. Martin Fleischmann
Department of Chemistry
University of Southampton
Southampton SO9 5NH
UNITED KINGDOM

Dr. H. Tachikawa
Chemistry Department
Jackson State University
Jackson, Mississippi 39217

Dr. John W. Wilkins
Cornell University
Laboratory of Atomic and
Solid State Physics
Ithaca, New York 14853

Dr. Ronald Lee
R301
Naval Surface Weapons Center
White Oak
Silver Spring, Maryland 20910

Dr. Robert Gomer
Department of Chemistry
James Franck Institute
5640 Ellis Avenue
Chicago, Illinois 60637

Dr. Horia Metiu
Chemistry Department
University of California
Santa Barbara, California 93106

Dr. W. Goddard
Department of Chemistry and Chemical
Engineering
California Institute of Technology
Pasadena, California 91125


DATE
FILMED
3 8